

# CONTROL OF SATELLITE FORMATIONS NEAR EARTH-MOON LAGRANGE POINTS FOR INTERFEROMETRIC CHARACTERIZATION OF CISLUNAR OBJECTS

Erin E. Fowler\* and Derek A. Paley†

This paper describes a formation selection and control scheme based on Bravais lattice configurations for interferometric imaging of other spacecraft in the cislunar regime by a spacecraft formation near a collinear Earth-Moon Lagrange point. The value of space-based interferometry for the cislunar space domain awareness mission is assessed using methods for formation control in three-body dynamics and metrics for interferometric imaging.

## INTRODUCTION

In geometry and crystallography, a Bravais lattice is an infinite array of discrete points that describe the possible configurations into which atoms can be arranged in crystals.<sup>1</sup> In three-dimensional space, there are fourteen Bravais lattices grouped into seven types, e.g., cubic, monoclinic, orthorhombic.<sup>1</sup> A fundamental aspect of any Bravais lattice is that for any choice of direction the lattice appears exactly the same from each of the discrete lattice points when looking in that direction.<sup>1</sup> In an equilibrium shaping strategy for autonomous distributed satellite swarm control, the choice of certain Bravais lattice configurations to define satellite positions in the swarm offers a reduced requirement for communication and coordination among the spacecraft while still safely achieving and maintaining the desired formation.<sup>2</sup> Choosing certain Bravais lattice configurations for cislunar spacecraft formations may also be beneficial for achieving desirable interferometric baselines with respect to a distant target.

This paper assesses the control of satellite formations in cubic, tetragonal, and hexagonal Bravais lattice configurations near collinear Earth-Moon Lagrange points and quantifies the tracking performance and control cost of these formation against distant cislunar targets. Previous research related to interferometric imaging by satellite formations in three-body dynamics describes a continuous feedback control algorithm that maintains a formation of satellites in motion bounded relative to a halo orbit in the Sun-Earth/Moon system and shows image reconstruction and  $(u, v)$  plane coverage for interferometric satellite configurations for astronomy applications.<sup>3</sup> Gurfil and Kasdin develop a time-varying continuous linear-quadratic control law for formation-keeping in the circular restricted three-body problem (CR3BP).<sup>4</sup> Previous work exists on the design of formations for interferometric collections in cislunar space;<sup>5</sup> this paper describes new formation configurations and extends the

---

\*PhD Candidate, Aerospace Engineering, University of Maryland College Park, Glenn L. Martin Hall, College Park, MD 20742.

†Willis H. Young Jr. Professor of Aerospace Engineering Education, Director, Maryland Robotics Center, Aerospace Engineering, The Institute for Systems Research, Electrical and Computer Engineering, Maryland Robotics Center, Brain and Behavior Institute, University of Maryland College Park, 3150 Glenn L. Martin Hall, College Park, MD 20742.

previous analysis to address the control of these formations near Lagrange points and the impact of the control scheme on the interferometric resolution produced by the proposed formation.

The cislunar regime is of increasing interest to the space industry due to its value for applications such as astronomy, interplanetary mission staging, lunar exploration and communications, and Earth orbit insertion. With the rising international interest in this regime and the expectation of increased traffic between the Earth and the Moon, strategies for improved space situational awareness (SSA) and space domain awareness (SDA) in this regime may become increasingly important. The chaotic dynamics that characterize cislunar space present significant challenges for spacecraft tracking and the large distances and sensor exclusion zones that characterize this regime complicate the use of traditional SDA solutions. Interferometry could be very valuable for space domain awareness and spacecraft characterization applications in the cislunar regime because it promises high resolution at large distances. Additionally, interferometry in the optical wavelengths, while previously considered an insurmountable spacecraft control challenge, may be possible with improved timing and time transfer technologies in the coming years.

The outline of this paper is as follows. The next section describes cislunar trajectories. Next we describe the placement of satellites in a formation according to a Bravais lattice configuration and a metric for  $(u, v)$  plane coverage. Improved  $(u, v)$  plane coverage should produce improved angular resolution and thus an improved tracking custody result. Lastly, we describe both open-loop and closed-loop  $(u, v)$  plane coverage results, identifying the trade-off that must be made between increasing the angular resolution produced by the interferometer and conserving station-keeping  $\Delta V$ .

## CISLUNAR TRAJECTORIES

In order to study the interferometric result that would be produced by a particular formation of satellites near Earth-Moon L2 against a particular target to be observed, we begin by choosing an epoch and initial conditions. The simulation begins at noon UTC on January 1, 2023. Inertial initial conditions for the target are provided in Table 1. We then choose the initial conditions for a reference or leader orbit for the formation orbiting Earth-Moon L2. Initial conditions for both target and interferometer reference orbit are identified as described by Grebow.<sup>6</sup> Figure 1 shows the non-dimensionalized motion in the Earth-Moon rotating frame of the formation reference trajectory and of the target object for fourteen days, the duration of the simulation. Previous research describes the dynamics of the Circular Restricted Three-Body Problem, the Earth-Moon rotating frame, and the constants for non-dimensionalization in the context of the cislunar regime.<sup>7</sup>

**Table 1:** Initial conditions for the target object and for the center of the interferometer formation, which orbits Earth-Moon L2.

Inertial Initial Conditions January 1, 2023, 12:00:00 UTC	Target	Interferometer Formation Orbiting EML2
$x$ (kilometers)	246,014.848	381,643.783
$y$ (kilometers)	187,454.216	290,798.449
$z$ (kilometers)	80,291.777	124,556.943
$vx$ (km/s)	-0.772	-0.517
$vy$ (km/s)	0.813	0.545
$vz$ (km/s)	0.470	0.315

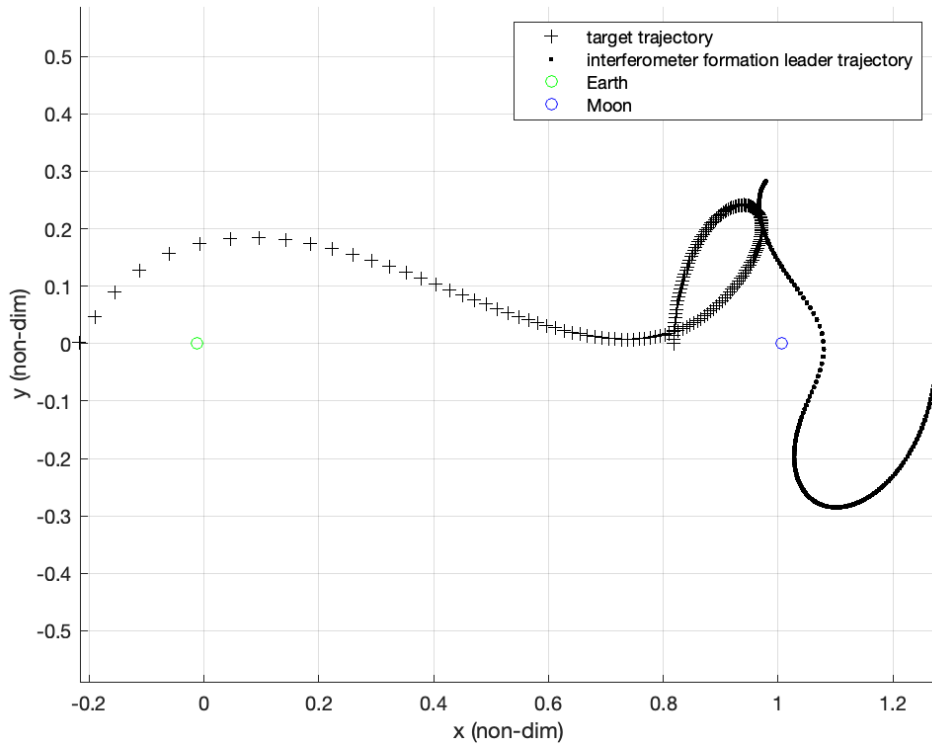


**Figure 1:** Trajectories for the target and interferometer formation reference, shown in the Earth-Moon rotating frame and in non-dimensionalized coordinates. The positions of the Earth and Moon are identified as green and blue circles.

## FORMATION DESIGN AND ANALYSIS

### Bravais Lattice as a Formation Design Tool

In three-dimensional space, there are fourteen Bravais lattices grouped into seven types.<sup>1</sup> Figure 2 identifies the edges and axial angles whose relationships to each other in the case of each type of three-dimensional lattice are defined in Table 2. Defining various Bravais lattices with different values for  $a$ ,  $b$ ,  $c$ ,  $\alpha$ ,  $\beta$ , and  $\gamma$ , positioning a satellite at each corner of a lattice, and centering these lattices around the formation reference trajectory identified in Table 1 and Figure 1 allows us to compare these lattices as interferometer designs for observations of a cislunar target. The formation-keeping method used to maintain these Bravais lattice configurations can be found in Gurfil and Kasdin.<sup>4</sup>

### $(u, v)$ Plane Coverage Metric

The van Cittert–Zernike theorem,<sup>8</sup> named after physicists Pieter Hendrik van Cittert and Frits Zernike, is a formula that states that under certain conditions the Fourier transform of the intensity distribution function of a distant, incoherent source is equal to its complex visibility, providing the basis for interferometric imaging. The theorem implies that if the value of the complex mutual coherence function is known at every point in the  $(u, v)$  plane, a two-dimensional Fourier transform may be used to create an image.<sup>9</sup> The van Cittert-Zernike result provides the following equation for the image of a source:<sup>3</sup>

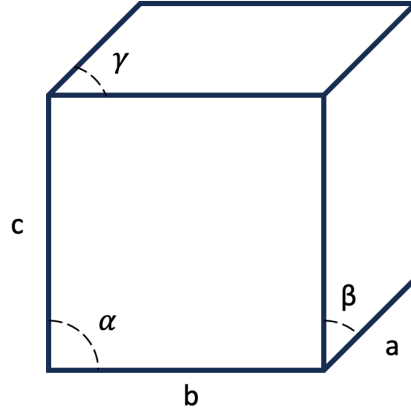


**Figure 2:** Edges  $a$ ,  $b$ , and  $c$ , as well as angles  $\alpha$ ,  $\beta$ , and  $\gamma$  are defined for the Bravais lattice families described in Table 2.

**Table 2:** Three-dimensional Bravais lattice families and their definition.

Crystal Family	Edge Lengths	Axial Angles
Triclinic		$\alpha \neq \beta \neq \gamma$
Monoclinic		$\alpha = \beta = \gamma = 90^\circ$
Orthorhombic		$\alpha = \beta = \gamma = 90^\circ$
Tetragonal	$a = b$	$\alpha = \beta = \gamma = 90^\circ$
Hexagonal	$a = b$	$\alpha = \beta = 90^\circ, \gamma = 120^\circ$
Hexagonal (rhombohedral)	$a = b = c$	$\alpha = \beta = \gamma$
Cubic	$a = b = c$	$\alpha = \beta = \gamma = 90^\circ$

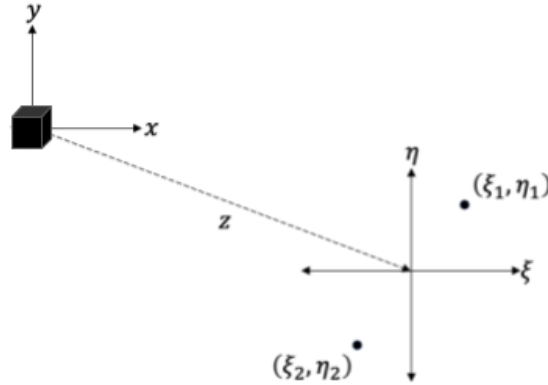


**Figure 3:** A depiction of the architecture of an interferometric imaging system, inspired by a similar figure in Howell and Millard 2009.<sup>3</sup> The target object is emitting or reflecting light of wavelength  $\lambda$  from the origin of the  $(x, y)$  plane. The formation is at distance  $z$  from the target. The positions of the satellites in the formation are projected into the  $(\xi, \eta)$  plane so that the spatial frequencies (points in the  $(u, v)$  plane) sampled by the interferometer can be calculated.

$$I(x, y) \approx \int_u \int_v \mu(u, v) e^{i2\pi(ux+vy)} dv du, \quad (1)$$

where  $\mu(u, v)$  is the complex mutual coherence function. The  $(u, v)$  plane, the plane of spatial frequencies sampled by an interferometer that are input to the mutual coherence function  $\mu$ , is a function of the position of the interferometer, its baselines, the wavelength sampled by the interferometer, and the target coordinates. Depicted in Figure 3, the  $(u, v)$  plane is defined by<sup>3</sup>

$$\begin{aligned} u_i(t) &= \frac{\eta_j - \eta_k}{z\lambda} \\ v_i(t) &= \frac{\xi_j - \xi_k}{z\lambda}, \end{aligned} \tag{2}$$

where  $\lambda$  represents the wavelength of light emitted or reflected by the target and collected by the interferometer. Here, numerical subscripts  $j$  and  $k$  indicate that position elements are associated with a particular spacecraft. Numerical subscripts  $i$  take values between 1 and  $\frac{2j!}{(j-2)!2!}$ , because two points in the  $(u, v)$  plane are measured for each baseline and there are as many baselines as pairs of spacecraft in the interferometer formation.<sup>10</sup> Because the amplitude associated with  $(u_i, v_i)$  is equal to the amplitude associated with  $(-u_i, -v_i)$ , one measurement by a pair of satellites (one baseline) in an interferometer produces two points on the  $(u, v)$  plane.<sup>10</sup>

The image of the source depends on  $u$  and  $v$ , which depend on the locations of the satellites in  $(\xi, \eta)$  space, according to Equation (2). If all points in  $(u, v)$  space, i.e. all spatial frequencies, can be sampled, then the complete image can be reconstructed by the interferometer. In the case of an interferometer with two telescopes of diameter  $D$  separated by a baseline vector  $\mathbf{B}$  defined in the  $(\xi, \eta)$  plane, the  $(u, v)$  plane consists of a low-frequency peak of extent  $\pm D/\lambda$  and two high-frequency peaks of extent  $\pm D/\lambda$  located at  $\pm \mathbf{B}/\lambda$ .<sup>11</sup> The interferometer acts thus as a high-frequency band pass filter, allowing it to reach information at a resolution of  $1.22\lambda/|\mathbf{B}|$ , outperforming a single telescope of diameter  $D$  with resolution  $1.22\lambda/D$ . An interferometer consisting of  $n$  telescopes produces  $\frac{n(n-1)}{2}$  baselines and thus samples  $\frac{n(n-1)}{2}$  frequencies in the Fourier transform of the brightness distribution of the object.<sup>11</sup>

A specific description of space-based interferometry is provided by Hussein: “Interferometric imaging is performed by measuring the mutual intensity ... that results from the collection and subsequent interference of two electric field measurements of a target made at two different observation points. While moving relative to each other, the satellites collect and transmit these measurements, which are later combined at a central node using precise knowledge of their locations and timing of data collection. A least squares error estimate of the image can be reconstructed given the mutual intensity measurements, parameters of the optical system, and the physical configuration of the observatory.”<sup>12</sup>

Given that the  $(u, v)$  plane coverage defines the sampling of the Fourier transform of the object brightness distribution, sparse sampling of the  $(u, v)$  plane is a common concern for interferometry as compared to single-dish observations. Sparse sampling results in lower signal-to-noise ratio (lower sensitivity). Noise magnitude is inversely proportional to the square root of the collection area of the telescopes, which would be  $n\pi(\frac{D}{2})^2$  for  $n$  telescopes of diameter  $D$  as described above.<sup>13</sup> As Chakrovorty points out, “the noise can be reduced by increasing the collection area of the telescopes. However,... costs (and other possible issues such as fuel usage) often dictate the size of the telescopes that can be put in space.”<sup>13</sup> While noise magnitude is dependent on the number of telescopes and the size of each, increased sampling of the  $(u, v)$  plane can be accomplished not only by increasing the number of telescopes or the size of each telescope, but also by changing the positions of the telescopes as projected onto the  $(\xi, \eta)$  plane. This motion of the telescopes in the plane or-

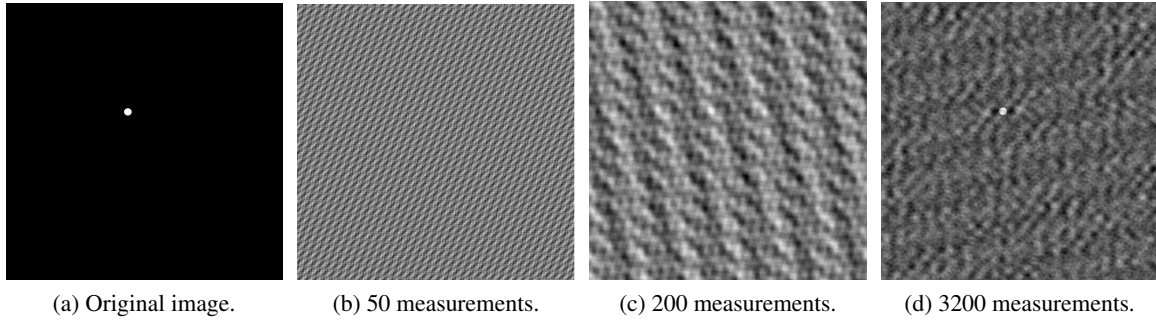


**Figure 4:** Simulated interferometric reconstruction of a  $800 \times 800$  pixel image of a point source based on randomly selected points on the  $(u, v)$  plane.

thogonal to the direction from the formation to the target allows sampling of unsampled frequencies in the  $(u, v)$  plane. As the target and individual telescopes in the interferometer move due to natural or forced-motion dynamics, baseline length and orientation change, resulting in measurements over different spatial frequencies and directions in the  $(u, v)$  plane for better image synthesis.

Figure 4 shows an improving image reconstruction as a function of increasing numbers of randomly sampled  $(u, v)$  points against a digital original image and exemplifies the importance of abundant sampling of the spatial frequencies in the  $(u, v)$  plane defined against a particular source. Because the interferometry application studied in this research is tracking a distant object in cislunar space, the details of that object need not be resolved, but the interferometer does need to sample enough spatial frequencies to precisely identify the angular location of the object on the celestial sphere as input to a state estimation algorithm used to track the object.

In designing a metric for  $(u, v)$  plane coverage, we identified two key qualitative points about the goodness of a sampling scheme:

1. For a multiple-element array, the best choice of relative positions for the elements in the array over time is that which most closely approximates uniform sampling of the  $(u, v)$  plane within a relevant area. The uniform sampling of spatial frequencies helps avoid degeneracies or aliasing in image reconstruction.<sup>14</sup>
2. The relevant area of the  $(u, v)$  plane can be identified once the intended mission for the interferometer is established. Interferometers can be optimized for various types of measurement, resulting in various  $(u, v)$  plane coverage metrics. For example, interferometers can be used for visibility measurements (detecting the size of an object), astrometry (detecting the position of an object), and imaging (detecting the structural details of an object). Long baselines measure information about the small-scale structure of the source but are insensitive to large-scale structure; conversely, short baselines measure information about the large-scale structure of the source but are insensitive to small-scale structure. In order to precisely measure the position of a target object (astrometry), baselines  $\mathbf{B}$  should be as long as possible without actually resolving the target.<sup>15</sup> Thus, in order to optimize the placement of telescope elements in an interferometer for a particular type of measurement against a target, some characteristics of the target must be estimated in advance of the measurement.

To analyze the  $(u, v)$  plane coverage of a particular satellite formation, coordinates in the Earth-

Moon rotating frame of the satellites relative to the reference L2 orbit are first transformed to the inertial frame and then projected into a plane perpendicular to the line-of-sight to the target. Coordinates in this perpendicular plane are  $(\xi, \eta)$  and coordinates on the  $(u, v)$  plane are calculated from  $(\xi, \eta)$  coordinates by Equation (2).

As previously discussed, a goal for a formation of satellites performing interferometry in order to produce astrometric observations, i.e., unresolved imagery used for precisely measuring the position of a target object rather than the structural details, is to maintain baselines that produce angular resolution very similar to the anticipated target object angular size. The following scalar metric, where  $P$  represents a distribution of points, describes the percentage of  $(u, v)$  plane points that are covered by the formation but are unnecessary for the desired measurement, where a lower value represents a better result:

$$c = \int \int |P_{ideal} - P_{formation}| dx dy \quad (3)$$

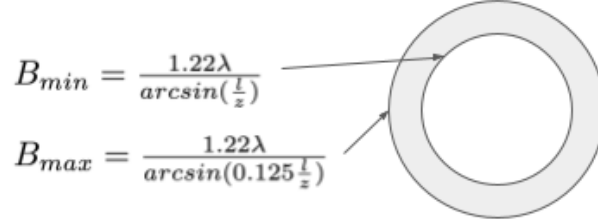


**Figure 5:** A depiction of the proposed  $(u, v)$  plane coverage metric.

Figure 5 provides a depiction of the metric  $c$ . Here,  $P_{ideal}$  is an annulus with the inner radius defined by the minimum baseline that produces a measurement of the target object of a certain size. The resolution of an interferometer in radians can be calculated as  $1.22\lambda/|\mathbf{B}|$  and the angular extent of a distant object in radians can be calculated as  $\arcsin(\frac{l}{z})$ . When the target angular size is smaller than the resolution of the interferometer, the target is not visible to the interferometer. On the other hand, if the target angular size is much larger than the resolution of the interferometer, an interferometer would only resolve structural details rather than precise position information. A successful formation creates evolving baselines over time which remain inside this annulus as often as possible and cover as many points in the annulus as possible.

In the examples studied for this analysis, we use a spherical target object of diameter four meters. For the interferometer to produce a resolution small enough to detect the target object, a pair of its satellites must create a minimum baseline size of  $B_{min} = \frac{1.22\lambda}{\arcsin(\frac{l}{z})}$ , where  $\lambda$  is the wavelength of light reflected by the target,  $l$  is the target size in meters, and  $z$  is the distance from the  $(\xi, \eta)$  plane in meters. Because our goal is not to resolve the structural details of the distant target, the diameter of the larger concentric circle of the annulus corresponds to a maximum baseline defined by  $B_{max} = \frac{1.22\lambda}{\arcsin(0.125 \frac{l}{z})}$ . Assume wavelength  $\lambda = 780$  nanometers, which represents the boundary between optical and near-infrared radiation. For distance  $z$ , we use an average distance between the reference EML2 orbit, which is the center of the formation comprising the interferometer, and the target for the duration of the measurement collection. The minimum baseline, i.e., the diameter of the inner concentric circle of  $P_{ideal}$ , produced as described above for an interferometer orbiting

EML2 and observing a four-meter spherical target reflecting energy at 780 nm wavelength from the target trajectory defined above, is 83 meters, while the maximum baseline, the diameter of the outer concentric circle of  $P_{ideal}$ , is 661 meters. These minimum and maximum baseline values inform choices of  $83 < a < 661$  meters and  $83 < c < 661$  meters shown in Table 3.

## INTERFEROMETRIC RESULTS

The motion of the target and individual telescopes in the interferometer due to natural or forced-motion dynamics causes changes in baseline length and orientation over time, resulting in measurements over different spatial frequencies, i.e., points in the  $(u, v)$  plane for image synthesis. Results provided in this section show the  $(u, v)$  plane coverage that is produced by natural motion, i.e., open-loop assessment with no station-keeping, as well as forced motion, i.e., closed-loop assessment, using station-keeping to maintain desired relative positions for the formation.

### Open-Loop Assessment: $(u, v)$ Plane Coverage Results for Uncontrolled Formations about Earth-Moon Lagrange Point L2

**Table 3:** Bravais lattice configurations considered in this analysis. Note: A Bravais configuration that includes only four nodes is actually two-dimensional; a three-dimensional cubic requires more than four nodes (satellites) in the formation.

Number of Satellites	Number of Baselines	Bravais Configuration (meters)
4	6	cubic ( $a = 100$ )
8	28	cubic ( $a = 100$ )
4	6	cubic ( $a = 650$ )
8	28	cubic ( $a = 650$ )
4	6	tetragonal ( $a = 100, c = 650$ )
8	28	tetragonal ( $a = 100, c = 650$ )
4	6	tetragonal ( $a = 650, c = 100$ )
8	28	tetragonal ( $a = 650, c = 100$ )
4	6	hexagonal ( $a = 100, c = 650$ )
8	28	hexagonal ( $a = 100, c = 650$ )
4	6	hexagonal ( $a = 650, c = 100$ )
8	28	hexagonal ( $a = 650, c = 100$ )

Table 3 displays the Bravais lattice configurations considered in this analysis. Each of these formations is considered, both as a closed-loop (station-kept) formation and as a starting condition for an open-loop formation, so that the satellites are allowed to drift according to the simulation dynamics without any maneuvers.

### Closed-Loop Assessment: $(u, v)$ Plane Coverage Results for Station-kept Formations about Earth-Moon Lagrange Point L2

Results depicted in Figure 10 indicate that closed-loop (station-kept) formations outperform open-loop formations in terms of the  $(u, v)$  plane coverage metric of % time within the annulus. This finding makes sense when the relative trajectories of station-kept formations are compared with those of the formations which are allowed to drift over the simulation time of fourteen days. Figures 6 and 7 depict the motion of the eight-satellite hexagonal Bravais lattice configuration with  $a = 650$  and  $c = 100$  without station-keeping, and Figures 8 and 9 show the same configuration

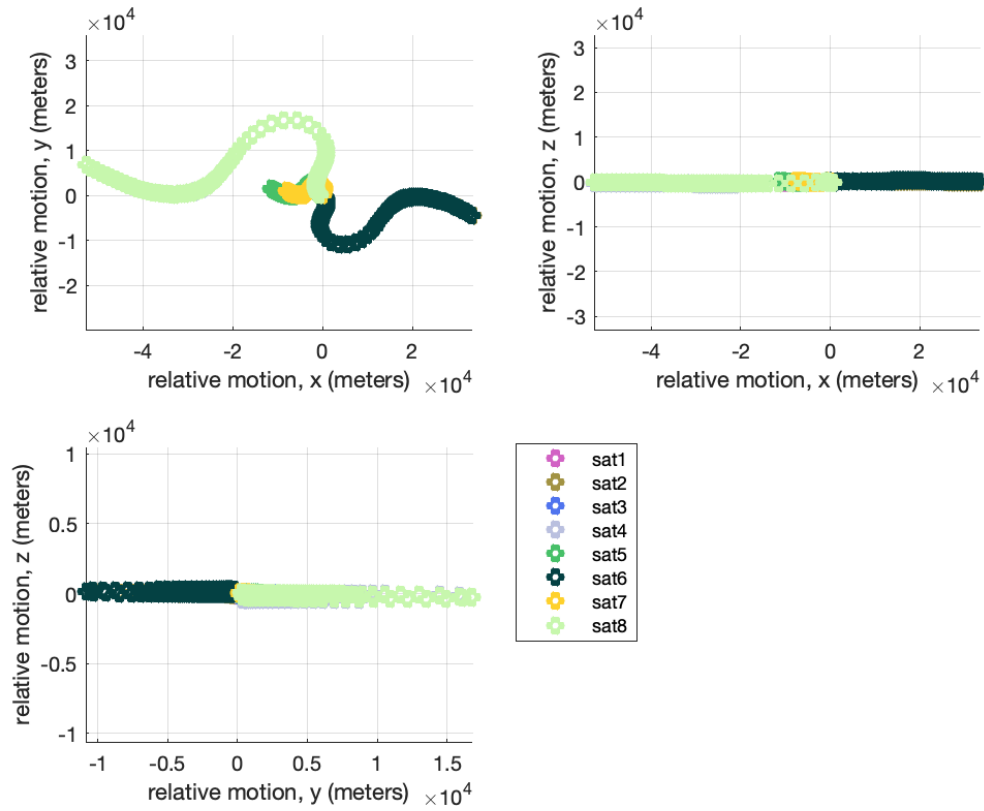


**Figure 6:** Open-loop propagation, shown in the rotating frame with the nominal L2 trajectory at the origin, for the eight-satellite hexagonal Bravais configuration with  $a = 650$  and  $c = 100$ .

with station-keeping for comparison. The satellites in a formation that are not station-kept drift away from each other over time, creating large baselines outside the annulus of desired points of coverage.

The closed-loop formations do not always outperform the open-loop formations in terms of the  $(u, v)$  plane coverage metric of % of annulus covered. In fact, the closed-loop formations only outperform the open-loop formations for this metric in the cases of the four- and eight-satellite tetragonal Bravais lattices with  $a = 650$  and  $c = 100$  and the four- and eight-satellite hexagonal Bravais lattices with  $a = 650$  and  $c = 100$ . The fact that the satellites in the open-loop formations are allowed to drift leads both to the result that the baselines at more time steps are outside the desired annulus and to the result that more points within the desired annulus are visited by the formation. The satellites in open-loop configurations drift apart over time, resulting in larger baselines outside the desired annulus over time. On the other hand, during the earlier part of the simulation, the fact that the satellites are allowed to drift means that they visit more points within the desired annulus early in the simulation time than the closed-loop alternative. Some of these formations may benefit from a station-keeping strategy that allows some drifting of the satellites within the desired annulus before maneuvers control their tendency to drift very far apart over the longer term. The station-keeping strategy simulated here includes a maneuver for each satellite every two hours.

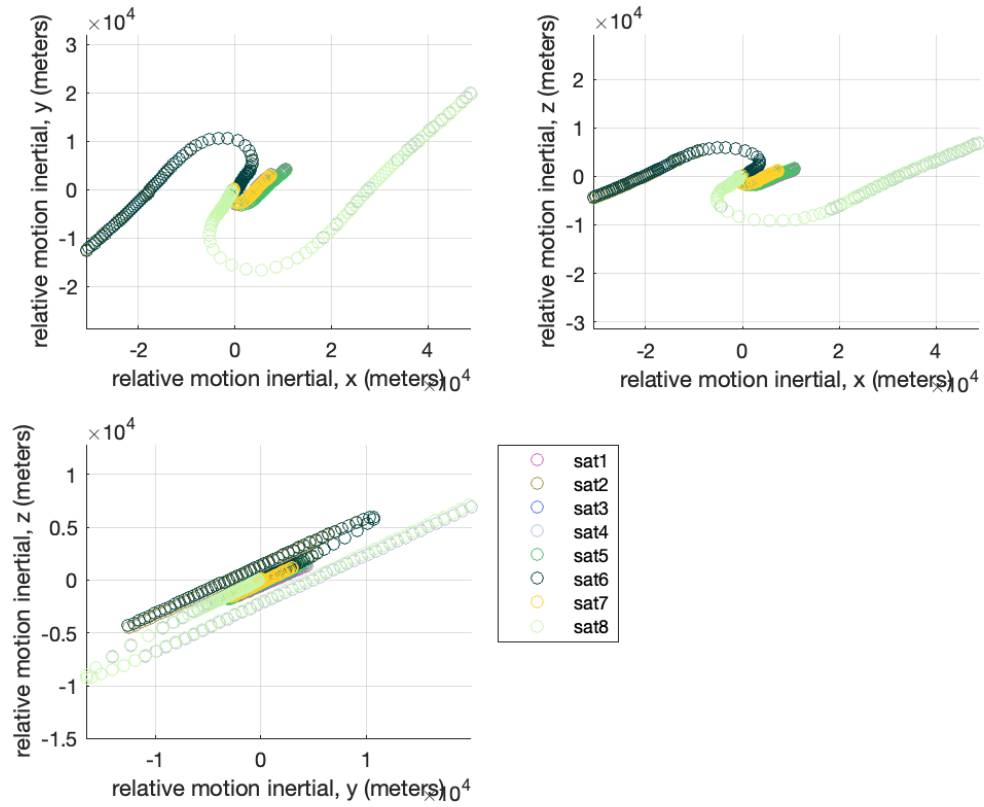


**Figure 7:** Open-loop propagation, rotated into the inertial frame and translated so that the nominal L2 trajectory is at the origin, for the eight-satellite hexagonal Bravais configuration with  $a = 650$  and  $c = 100$ .

The closed-loop eight-satellite tetragonal Bravais lattice with  $a = 650$  and  $c = 100$  and the closed-loop eight-satellite hexagonal Bravais lattice with  $a = 650$  and  $c = 100$  are the best formation choices for the target studied here. These two station-kept formations outperform their open-loop counterparts for both  $(u, v)$  plane coverage metrics and outperform the other formation choices studied here.

## CONCLUSION

The  $(u, v)$  plane coverage analysis performed on various Bravais lattice configurations for a free-flying interferometer near Earth-Moon L2 indicates that an interferometer can provide higher resolution collections than a single telescope and identifies the two highest-performing configurations against the chosen target. These findings motivate further research into free-flying interferometry for SSA and SDA applications. Interferometry is traditionally a technique used for astronomy applications with much more distant targets as compared to the artificial satellites and debris that are targets for SSA and SDA applications, so interferometry algorithms would need to be updated to accommodate observations of targets at 10,000 – 100,000 km rather than effectively infinitely distant targets.

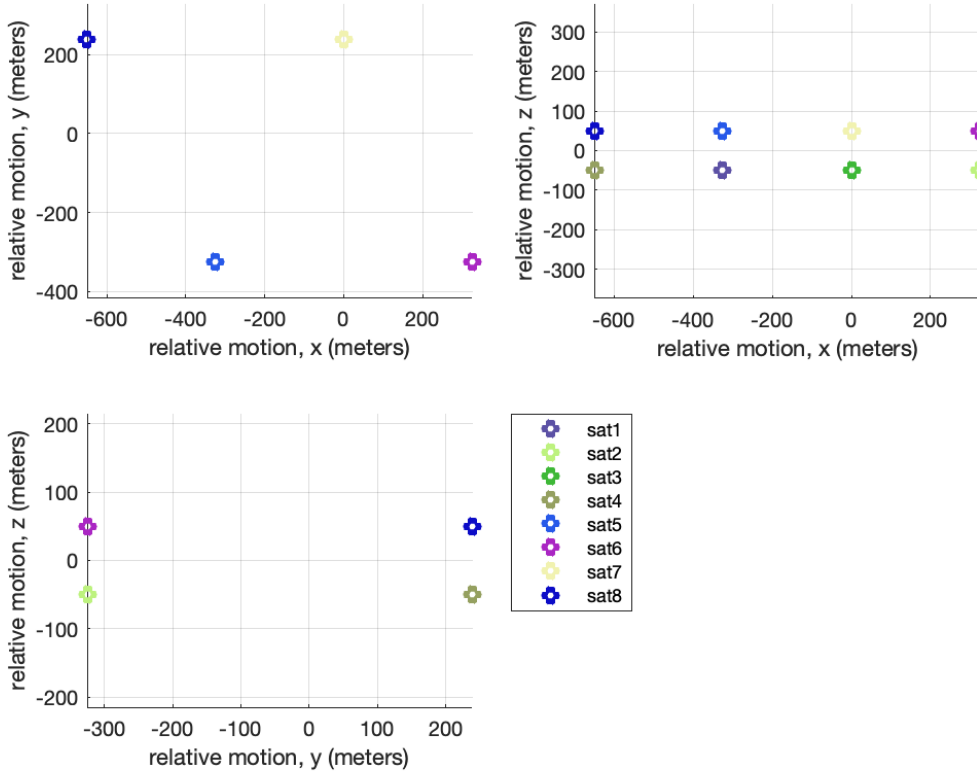


**Figure 8:** Closed-loop (station-kept) propagation, shown in the rotating frame with the nominal L2 trajectory at the origin, for the eight-satellite hexagonal Bravais configuration with  $a = 650$  and  $c = 100$ .

A benefit to flying a space-based optical long-baseline interferometer is that it removes the requirement for ground-based interferometers to rapidly and constantly monitor atmospheric effects, but an obstacle for a space-based free-flying interferometer performing direct detection (homodyne) interferometry at optical wavelengths is the requirement for extremely precise relative position control, within a wavelength of the sampled light.<sup>16</sup> While less sensitive than direct detection interferometry, heterodyne interferometry allows this requirement for precise position control to be safely neglected in favor of precise position and timing knowledge among interferometer elements, allowing for the use of a “widely dispersed, loosely organized ‘swarm’ of functionally identical spacecraft-borne optics,” with formation-keeping precision similar to that simulated in this paper, to perform the desired mission based on the use of a “precise metrology system and large-scale, parallel signal processing to perform interferometric imaging without the requirement of precise inter-spacecraft positioning and alignment control.”<sup>17</sup> We argue that interferometry in the optical wavelengths, while previously considered an insurmountable spacecraft control challenge due to the assumption that homodyne methods would be required, may be possible with heterodyne methods combined with improved timing and time transfer technologies in the coming years.

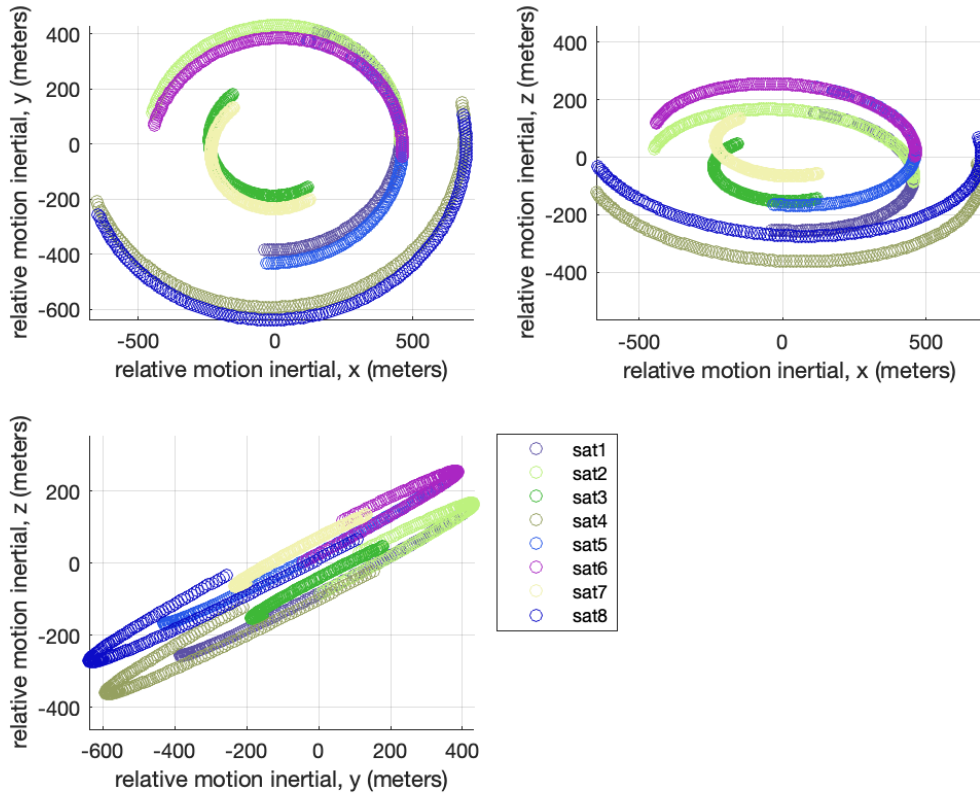


**Figure 9:** Closed-loop (station-kept) propagation, rotated into the inertial frame and translated so that the nominal L2 trajectory is at the origin, for the eight-satellite hexagonal Bravais configuration with  $a = 650$  and  $c = 100$ .

## ACKNOWLEDGMENT

This work was supported in part by the Johns Hopkins Applied Physics Laboratory’s Part Time Study Program.

## REFERENCES

- [1] C. Kittel, *Introduction to Solid State Physics*. Wiley, 2004.
- [2] D. Izzo and L. Pettazzi, “Autonomous and Distributed Motion Planning for Satellite Swarm,” *Journal of Guidance, Control, and Dynamics*, Vol. 30, No. 2, 2007.
- [3] K. H. Howell and L. D. Millard, “Control of Satellite Imaging Formations in Multi-Body Regimes,” *Acta Astronautica*, Vol. 64, 2009, pp. 554–570.
- [4] P. Gurfil and N. J. Kasdin, “Stability and control of spacecraft formation flying in trajectories of the restricted three-body problem,” *Acta Astronautica*, Vol. 54, 2004, pp. 433–453.
- [5] E. E. Fowler and D. A. Paley, “Formation Flight Design Near Earth-Moon Lagrange Points for Interferometric Characterization of Cislunar Objects,” Proceedings of the Advanced Maui Optical and Space Surveillance Technologies Conference, 2023.
- [6] D. J. Grebow, “Generating Periodic Orbits in the Circular Restricted Three-Body Problem with Applications to Lunar South Pole Coverage,” Master’s thesis, Purdue University, West Lafayette, IN, May 2006.

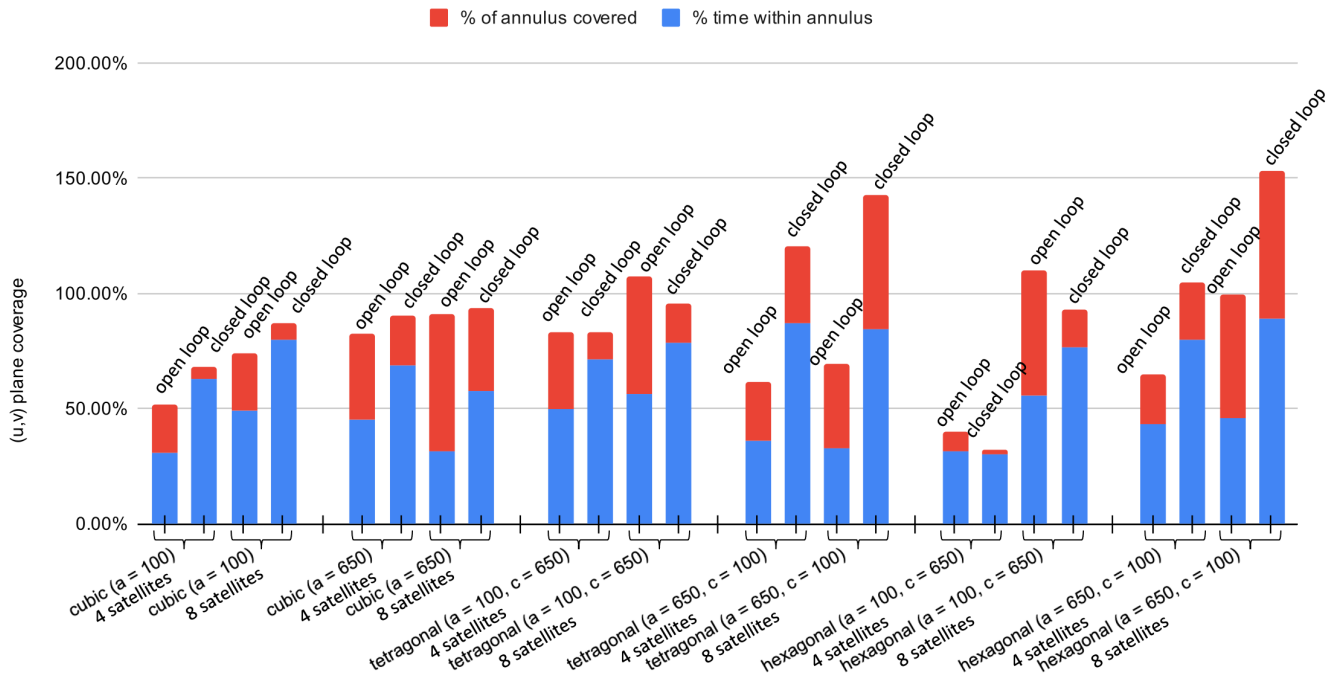


Figure 10: Open- and closed-loop results for formations described in Table 3.

- [7] E. E. Fowler and D. A. Paley, “Observability Metrics for Space-Based Cislunar Domain Awareness,” *Journal of the Astronautical Sciences*, April 2023, 10.1007/s40295-023-00368-w.
- [8] F. Zernike, “The Concept of Degree of Coherence and Its Application to Optical Problems,” *Physica*, Vol. 5, August 1938, pp. 785–795, 10.1016/S0031-8914(38)80203-2.
- [9] L. Millard and K. Howell, “Control of interferometric spacecraft arrays for (u, v) plane coverage in multi-body regimes,” *Journal of Astronautical Sciences*, Vol. 56, January–March 2008.
- [10] L. D. Millard, *Control of Satellite Imaging Arrays in Multi-Body Regimes*. PhD thesis, Purdue University, West Lafayette, IN, May 2008.
- [11] D. Mourard, “Optical Long Baseline Interferometry: Examples from Vega/Chara,” *New Concepts in Imaging: Optical and Statistical Models*, Vol. 59, 2013, pp. 25–36.
- [12] I. Hussein, D. Scheeres, and D. Hyland, “Control of a Satellite Formation For Imaging Applications,” *American Control Conference*, July 2003, 10.1109/ACC.2003.1238958.
- [13] S. Chakravorty, P. Kabamba, and D. Hyland, “Modeling of Image Formation in Multi-Spacecraft Interferometric Imaging Systems,” *AIAA Space Conference*, No. 5895, San Diego, California, September 2004.
- [14] D. Woody, “ALMA Configurations with complete UV coverage,” Tech. Rep. 270, California Institute of Technology Owens Valley Radio Observatory, Big Pine, CA, August 1999.
- [15] F. Millour, “Interferometry concepts,” *EAS publication series*, Vol. 69-70, 2015, 10.1051/eas/1569003.
- [16] J. Wachs, J. Lee, R. Linfield, J. Kommers, and W. Cash, “Spectrally Resolved Synthetic Aperture Imaging Interferometer,” Tech. Rep. 17-NIAC18B-0145, Ball Aerospace, January 2019.
- [17] D. Hyland, “Interferometric imaging concepts with reduced formation-keeping constraints,” *AIAA Space Conference*, Albuquerque, New Mexico, August 2001.